Fluoride ion disorder and clustering in superionic PbF_2

2001 J. Phys.: Condens. Matter 13 9963

(http://iopscience.iop.org/0953-8984/13/44/311)

INSTITUTE OF PHYSICS PUBLISHING JOURNAL OF PHYSICS: CONDENSED MATTER

J. Phys.: Condens. Matter **13** (2001) 9963–9983 PII: S0953-8984(01)23063-X

Fluoride ion disorder and clustering in superionic PbF_2

Michael J Castiglione and Paul A Madden

Physical and Theoretical Chemistry Laboratory, Oxford University, South Parks Road, Oxford OX1 3QZ, UK

Received 19 March 2001, in final form 8 August 2001
Published 19 October 2001
Online at stacks.iop.org/JPhysCM/13/9963

Abstract

Computer simulations of the β-phase of PbF_2 using a polarizable ion interaction potential are described. Studies of KF- and YF_3-doped PbF_2, as well as the pure material are included. The simulations reproduce the macroscopic observables associated with the transition to superionic behaviour well, including the heat capacity, lattice constant and conductivity. An explanation is provided of the familiar observation of the similarity of the conductivities of the superionic solid just below and of the melt just above the melting transition. Comparisons are made with diffraction and diffuse scattering studies, which confirm that the nature of the fluoride ion disorder above the transition temperature in the simulations is very similar to that deduced from experiments. This involves a cooperative excitation of the fluoride sublattice, which results in the creation of a large number of vacancies and interstitials. Detailed studies of the positional correlations between these defects reveal a high degree of order associated with specific clustering effects. These positional correlations appear to be stronger than would be anticipated from recent mean-field descriptions of the interactions between charged defects in superionic materials. The nature of the correlations is compared with that associated with the interstitial clusters found in moderately YF_3-doped PbF_2 at low temperatures.

1. Introduction

Lead fluoride is one of a number of systems of stoichiometry MX_2 that adopt the cubic fluorite crystal structure and which exhibit anion fast-ion conduction [1]. In the fluorites, the transition to superionic behaviour is a continuous one ('type-II') and is not associated with any structural change of the immobile lattice. Rather, the rate of increase of the conductivity with increasing temperature [2] picks up in the vicinity of a temperature T_c (702 K for PbF_2) at which there is also a peak in the heat capacity [3] and an increase in the lattice parameter [4]. At higher temperatures (but still well below melting) the conductivity saturates at about

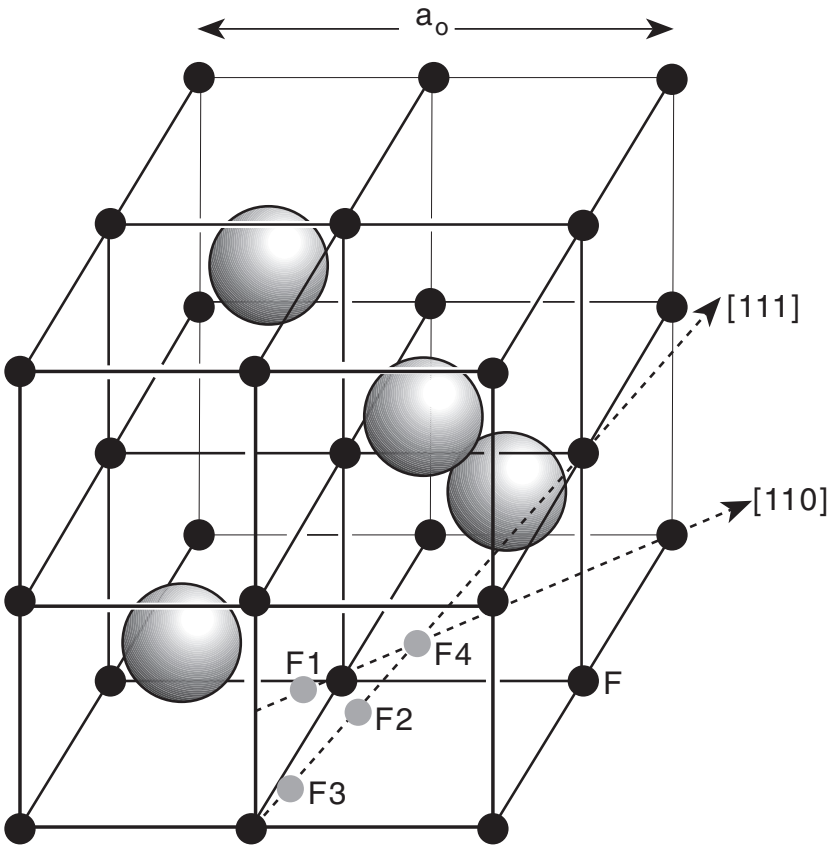

Figure 1. An illustration of the fluorite structure, showing the positions of the F(1), F(2) and F(4) interstitial sites which have sometimes been invoked in crystal structure refinements. These occur at F(1)–48i($\frac{1}{2}$, u, u), with $u \sim 0.36$; F(2)–323f(v, v, v), with $v \sim 0.4$; F(3)–32f(w,w,w), with $w \sim 0.31$; F(4)–4b($\frac{1}{2}$, $\frac{1}{2}$, $\frac{1}{2}$)—the classical octahedral site. The F(3) site in our analysis is not distinguished from a large amplitude oscillation about the F(1) site.

the same value as achieved in the melt [2]. At low temperatures ($<T_c$) the behaviour of the conductivity is consistent with the thermal excitation of isolated Frenkel pairs and the mobility of the vacancies and interstitials thus formed [1]. As illustrated in figure 1, one of the features of the fluorite lattice is the large, empty space about the octahedral site, denoted F(4). This is certainly large enough to accommodate interstitials, and this has been presumed to be the reason for the prevalence of superionic behaviour in fluorite-structured materials [1, 5]. The situation may be contrasted with the cotunnite (α) phase of PbF_2, which has a very similar energy to the β form [6] but which is not superionic. The cotunnite structure does not readily accommodate interstitials [7].

Low levels of aliovalent doping of β-PbF_2, e.g. with either KF or YF_3, increase the conductivity in the temperature domain below T_c [2, 8]. The K^+ or Y^{3+} ions substitute for Pb^{2+} on the normal cation sites and a fluoride vacancy or interstitial (respectively) is introduced. However, the temperature dependence of the conductivity and heat capacity around T_c in the doped and undoped materials indicates that a collective effect comes into play at this

temperature and swamps the additional conductivity introduced by low levels of aliovalent doping.

The nature of this collective effect has been a matter of controversy for several years and it is with this that the present work is concerned. Recently, Maier and co-workers [9, 10] have explored the predictions of a simple model of interactions between a finite concentration of point defects introduced by Frenkel pair excitation. A similar model had earlier been proposed by Hyland [11]. The model allows for the defect concentration (c)-dependent screening of the Coulombic interactions between defects and, in a mean-field treatment, lowers the free energy with a term which scales as $c^{1/3}$. The theory predicts a sharp increase in the number of defects close to some critical temperature and a heat capacity anomaly of similar appearance to that observed experimentally [9, 11]. The nature of the disordering of the F^- ions in a number of fluorite-structured fluorides has been studied by neutron scattering, notably by Hutchings and co-workers [4, 12, 13]. These studies seem to show the consequences of more specific defect interactions than are included in the simple mean Coulomb-field description. The diffraction data and diffuse scattering are consistent with the formation of vacancy and interstitial clusters which extend over several unit cells. The interstitial site is not the classical octahedral hole F(4); rather the F(2) and F(1), illustrated in figure 1, are found to be occupied. Other F^- ions in the vicinity are also displaced from their regular lattice sites. Around T_c the number of these vacancies rapidly increases to about a quarter of all F^- ions [4]: at higher temperatures this value saturates, presumably due to (repulsive) interactions amongst the defect clusters.

Computer simulations with effective pair potentials have reproduced (semi-quantitatively) the observed behaviour of the conductivity [10, 14] and heat capacity [10]. However, they have not shown consistency with the observed structural information or contributed to the elucidation of the nature of the defect interactions. The most extensive studies of these aspects of fluorite-structure materials have been made by Jaccucci and Rahman [15] and by Gillan [16, 17] on CaF_2. Both groups reported a much smaller number of vacancies than observed experimentally and a very different structure for the disordered state than deduced from the diffuse scattering studies. In particular, they found no evidence for any long-lived fluoride site other than the regular lattice site.

In the present work we shall examine the fluoride disorder in pure β-PbF_2 as well as in KF- and YF_3-doped systems and make detailed comparisons with the experimental information, including the diffuse scattering. In previous MD simulation work on PbF_2, empirically parametrized, 'rigid ion' effective pair potentials have been used, in which polarization (and other possible many-body) effects are subsumed within the effective interaction parameters. A consequence of this is that the pair potential parameters acquire unphysical values if viewed as properties of true pair interactions; in particular, the C_6 'dispersion' parameter for the F–F interactions in CaF_2 and PbF_2 were found to be about six times greater than could be justified on an *ab initio* basis [18, 19]. In the simulations with effective potentials, this enhanced F–F attraction promotes F^- ion disorder, leading to superionic behaviour. In a realistic ionic potential, this effect appears to be attributable to the polarization effects. The polarizable potential used here has already been shown to describe a number of the properties of PbF_2 successfully [7, 19], including the phonon dispersion curves of the β-phase and ionic mobility in the α-phase. The polarization of the Pb^{2+} ion has been shown to have an important influence on the ionic motion and also on the predicted transition pressure to the α-phase. An advantage of using a realistic potential is that it is transferable, permitting comparisons with related materials, such as the highly conducting $PbSnF_4$ [20], without changing the Pb–F interaction parameters.

2. Simulation details

The interaction potentials for all interactions involving Pb^{2+}, F^- and K^+ have been specified in previous work [19]. The interaction model includes full, formal charges on the ions, and the Pb^{2+}, K^+ and F^- ions have their full, in-crystal polarizabilities [21, 22]. Wherever possible *ab initio* calculations [23] are used to parametrize sections of the model unambiguously. The Y^{3+} ion is treated as a triply charged, polarizable species ($\alpha_{Y^{3+}} = 4.1$ au). The same potential is used to describe its short-range interactions with F^- and Pb^{2+} as for the K–F and K–Pb interactions, since these are not crucial to the properties of interest.

All the calculations described below were performed on systems containing 108 cations. In the initial configurations of the doped systems, dopant cations were substituted for randomly selected Pb^{2+} ions, and the resulting vacancies (KF) or interstitials (YF_3) were placed on randomly selected F^- lattice sites or on the octahedral sites, respectively. The simulations were equilibrated at the desired statepoint for 120 ps and statistics gathered in a subsequent 120 ps run. Most calculations were equilibrated at constant pressure and subjected to Nosé–Hoover thermostats, using the algorithms suggested in [24].

A central part of our simulation analysis involves the assignment of F^- ions to either the normal site of the fluoride lattice, or to the other interstitial positions that they may visit. The assignment must be fairly robust, to cope with the high degree of vibrational motion which the ions exhibit at the temperatures of interest. To assign an ion to a site if it is within some spherical region about the position of the site in the stationary lattice is not sufficient. A convenient method [7], which exploits the fact that the Pb^{2+} ions do not exchange positions during the course of the run (see below), is to assign an ion to a tetrahedral site if it is within the tetrahedron whose vertices are formed by the instantaneous positions of the Pb^{2+} ions which surround that site in the stationary lattice. The F^- ion is inside the tetrahedron if the vectors joining it to two of the vertices have negative scalar products with the normals to the three planes in which each of the vertices lie. An ion which is not within any such a tetrahedral site is said to be interstitial. Any empty tetrahedral site is said to contain a vacancy. It is not meaningful to attempt to distinguish between the interstitial sites identified from crystallographic refinements (figure 1) at the high temperatures at which the superionic behaviour is observed.

3. Bulk properties of pure and lightly doped systems

We begin by presenting simulation results for the heat capacity, lattice parameter, diffusivity and conductivity in pure β-PbF_2 and in samples lightly doped ($\sim$1%) with KF and YF_3 in order to establish the relationships between the simulated and real systems as regards these bulk properties.

3.1. Heat capacity

The heat capacity of type-II superionic materials exhibits a peak as a function of temperature, sometimes referred to as a 'Bredig' transition [11]. Since change in the conductivity is continuous, this is the best way of assigning a transition temperature to the superionic domain. The heat capacity is estimated from the differences between the internal energies of simulations performed at intervals of 25 K. Since the simulations are performed at constant pressure, this gives a measure of C_p. Results for simulations of the pure material and for 1% KF- and YF_3-doped samples are shown in figure 2. They show a peak for the pure material at a temperature of

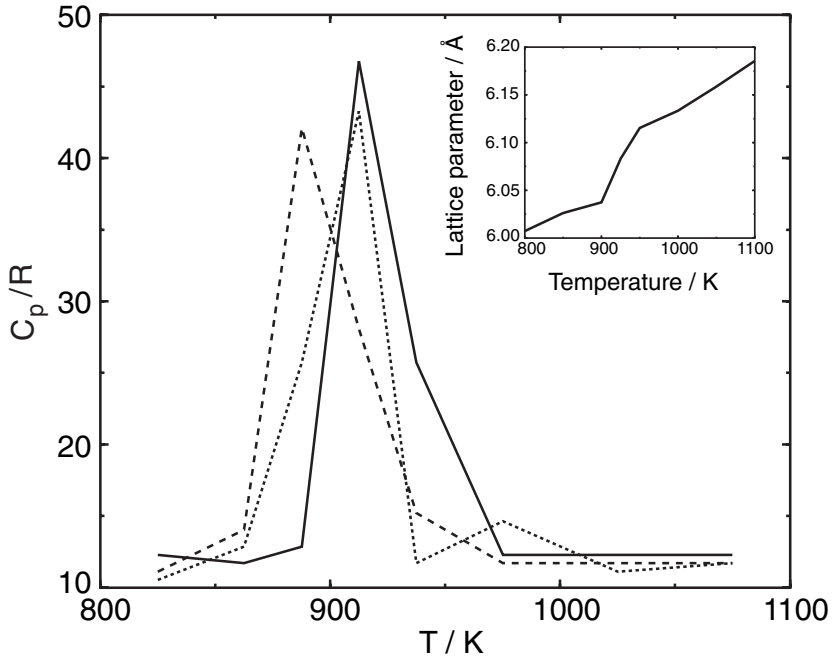

Figure 2. The heat capacities calculated for simulations of pure β-PbF_2 (solid line) and for 1%-doped samples with KF (dashed line) and YF_3 (dotted). Also shown (inset) is the lattice parameter.

910 K, which rises by about 32 R (∼0.27 kJ mol^{-1} K^{-1}) above the background. Experimentally [3], the peak appears at 702 K; this difference, of 200 K in the transition temperature, reflects a limitation of the simulation potential. The height of the experimental peak is about 20 R, but this difference (and the different shapes of the simulated and experimental curves) may reflect, in part, the crudeness of the numerical derivative we have used to estimate the heat capacity. From the area under the heat capacity peak, we may estimate the entropy change associated with the superionic transition

$$\Delta S = \int^{\text{peak}} \mathrm{d}T \frac{C_p}{T} \tag{3.1}$$

which gives a value of 12 J K^{-1} mol^{-1}.

The doped samples give heat capacity peaks of similar shape and height to the pure sample, which indicates that the change in F^- order at the transition is not strongly affected by the presence of the point defects. However, in the KF-doped system the peak has shifted to significantly lower temperatures (by ∼30 K). This indicates that the presence of the extrinsic vacancy in the sample has facilitated the F^- disordering. The experimental data on the conductivity of KF-doped PbF_2 [2] also suggest a shift to lower temperatures in the transition temperature.

3.2. Lattice parameter

The simulated system shows a sharp change in the mean lattice parameter as the temperature varies across the transition region (see figure 2 (inset)). This change is quite similar to that

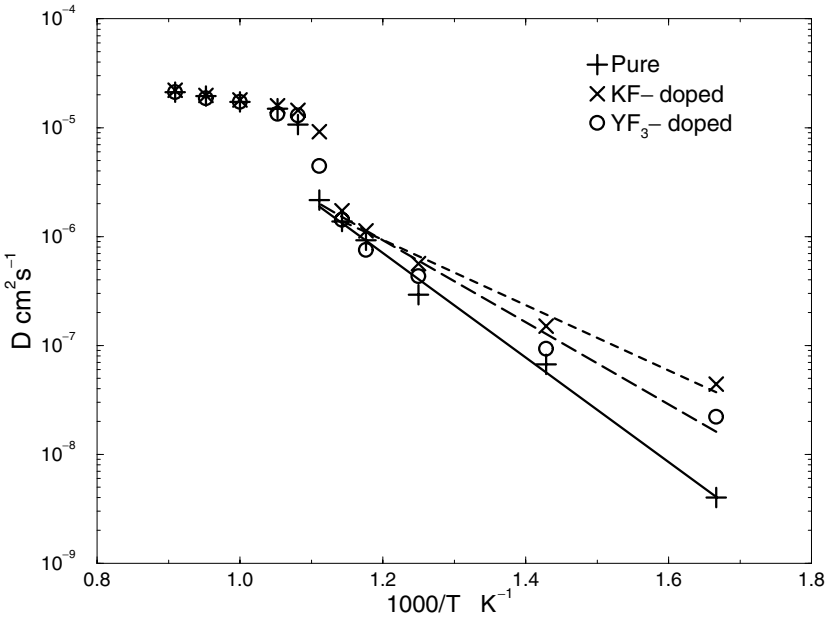

Figure 3. Arrhenius plots of the ionic diffusivities calculated for the pure (+) and 1% KF (×) and YF_3 (○) doped PbF_2 samples. Note the doping-induced enhancement of diffusivity below the transition temperature and the close similarity of the diffusivities in all samples above it.

observed in diffraction experiments [4]. The expansion across the transition (i.e. the difference between the extrapolated low and high temperature lines) is about 0.3 Å, whereas in the experiments it is about 0.2 Å. As with the heat capacity, this indicates a slightly bigger effect than that seen experimentally, to which the small system size may be a contributory factor.

3.3. Diffusivity

The diffusion coefficient may be calculated from the long time slope of the mean-squared displacement of the fluoride ions, i.e.

$$D = \lim_{t\to\infty} \frac{\langle |\,\delta \boldsymbol{r}_1(t)\,|^2 \rangle}{6t} \tag{3.2}$$

where $\delta \boldsymbol{r}_1(t)$ is the displacement of a typical fluoride ion in time t. In practice 'long-time' means over the range 30–50 ps. Examples of such mean-squared displacement curves appear below. The mean-squared displacements reveal a marked effect of aliovalent doping on the ionic mobility below the transition temperature, but essentially no effect above it. This is confirmed by plotting the diffusivities of the pure and 1% doped samples versus $1/T$ in figure 3. The enhancement of diffusivity below the transition temperature is due to the introduction of vacancies and interstitials by KF and YF_3 doping, respectively. Above the transition, it appears that this effect is swamped by ionic mobility associated with the F^- disorder. Note too that after the rapid rise of the diffusivity in the transition region, it plateaus and acquires a very slow temperature variation. This plateau persists over a temperature interval of more than 200 K before the simulated sample melts.

The behaviour revealed by the temperature dependence of the diffusivities is (at least) qualitatively consistent with that of the experimentally observed conductivity in doped and

pure PbF_2. Measurements on KF-doped samples over a wide range of compositions and temperatures have been made by Hull *et al* [2] and Liang and Joshi [8] measured the conductivity of YF_3 (and KF) doped samples below T_c. As well as 'swamping' of the extrinsic vacancy effect above T_c the KF measurements also show that the low temperature enhancement of conductivity by doping saturates for doping levels above about 2%, presumably as a consequence of vacancy–vacancy interactions. The simulated diffusivities exhibit the same behaviour.

From the Arrhenius plots of the diffusivities in figure 3 we can extract some information on the energetics of the diffusion process in the different samples below T_c. In this temperature domain, the behaviour of the diffusivity exactly parallels that of the ion-hopping rates extracted from a time-dependent analysis of the F^- site occupation, as described in detail in [7]. For the pure material we obtain an activation energy of about 95 kJ mol^{-1} (i.e. 1 eV). Given that diffusion in the pure material requires Frenkel pair formation, and since this is likely to be the rate-determining step of diffusion, we interpret this activation energy as the effective Frenkel pair formation energy in the simulated sample for temperatures of the order of 700–800 K. We can also estimate (crudely) the activation energies for vacancy and interstitial migration from the results for the doped samples. At the temperatures of the simulations, a significant number of the ion hops observed in these samples will be due to the intrinsic (Frenkel pair) mechanism. We therefore estimate the number of hops associated with the presence of the extrinsic vacancy or interstitial in the doped samples, by removing the estimated number of intrinsic hops from the total, and then subjecting the remaining hops to an Arrhenius analysis. This gives vacancy and interstitial migration energies of 45 and 48 kJ mol^{-1} respectively.

3.4. Conductivity—evidence of collective effects

Electrical conductivity is only directly related to the ion-hopping rate and diffusion coefficient if the motion of different ions is uncorrelated. We have examined this assumption and found significant differences between the degree of interionic correlations in the superionic crystal and liquid.

3.4.1. Conductivity calculation—method. Quite generally, the ionic conductivity is calculable as an integral over the charge current correlation function [25]

$$\lambda^K = \frac{\beta e^2}{V} \int_0^\infty J(t)\,\mathrm{d}t \tag{3.3}$$

where $\beta = 1/kT$, e is the electronic charge and J is

$$J(t) = \sum_{i=1}^{N}\sum_{j=1}^{N} Q_i Q_j \langle \boldsymbol{v}_i(t) \cdot \boldsymbol{v}_j(t)\rangle \tag{3.4}$$

$$= \sum_{i=1}^{N} Q_i^2 \langle \boldsymbol{v}_i(t) \cdot \boldsymbol{v}_i(0)\rangle + \sum_{j=1}^{N}\sum_{i\neq j}^{N} Q_i Q_j \langle \boldsymbol{v}_i(t) \cdot \boldsymbol{v}_j(0)\rangle \tag{3.5}$$

with Q_i and $\boldsymbol{v}_i$ the charge and velocity of each ion. The conductivity therefore involves the relative motion of the cations and anions. It is much more difficult to calculate than the diffusion coefficient as it is a collective quantity, so that converging the integral in the equation involves very long runs. A frequently used approximation is to neglect all the correlations in

the velocities of different ions, which leads to the so-called Nernst–Einstein relationship for conductivity

$$\lambda^{\mathrm{NE}} = \beta e^2(\rho_+ Q_+^2 D_+ + \rho_- Q_-^2 D_-) \tag{3.6}$$

where ρ_α and D_α are the number density and diffusion coefficient of species α. For an anion superionic conductor D_+ is zero, giving the normally assumed relationship between conductivity and anion diffusivity [1].

It is convenient to re-express the conductivity in the form of a mean-square displacement to make clear the problems of converging the integral in equation (3.3). This expression is

$$\lambda^K = \frac{\beta e^2}{V} \lim_{t\to\infty} (6t)^{-1} \left\langle \left| \sum_i Q_i \, (\delta \boldsymbol{r}_i(t)) \right|^2 \right\rangle \tag{3.7}$$

as can be shown by substituting

$$\delta \boldsymbol{r}_i(t) = \int_0^t \mathrm{d}\tau \; \boldsymbol{v}_i(\tau) \tag{3.8}$$

and using the stationarity of the correlation function to complete the integral ([25] p 201). Equation (3.7) can be written in the form

$$\lambda = \frac{\beta e^2}{V} \lim_{t\to\infty} (6t)^{-1} \langle | Q_+ \boldsymbol{\Delta}_+(t) + Q_- \boldsymbol{\Delta}_-(t)|^2 \rangle \tag{3.9}$$

where $\boldsymbol{\Delta}_\alpha(t)$ is the *net* displacement of all the ions of species α in time t

$$\boldsymbol{\Delta}_\alpha(t) = \sum_{i\epsilon\alpha} \delta \boldsymbol{r}_i(t). \tag{3.10}$$

Thus a plot of the mean-squared displacement appearing in the angle brackets versus time, should become linear after the short-time correlations have died out and the conductivity can be calculated from this slope. This equation makes it clear (bearing in mind the opposite signs of the cation and anion charges) that the conductivity involves the displacement of the set of anions relative to the set of cations. The Nernst–Einstein approximation can be written in an equivalent form:

$$\lambda^{\mathrm{NE}} = \beta e^2 \lim_{t\to\infty} (6t)^{-1} [Q_+^2 \rho_+ \langle |\delta_+(t)|^2 \rangle + Q_-^2 \rho_- \langle |\delta_-(t)|^2 \rangle] \tag{3.11}$$

where $\delta_\alpha(t)$ is the displacement of a *single* ion of species α.

3.4.2. Conductivity—results. We have calculated the collective conductivity for comparison with the Nernst–Einstein value at two temperatures which bracket the melting transition of the simulated material. Calculations were carried out at 1300 K (solid) and 1400 K (liquid). In both cases the simulations were first equilibrated at zero pressure and then the runs continued at the zero pressure density while the statistics on the particle displacements were accumulated. Results for the mean-squared displacements required in equations (3.11) and (3.9) are shown in figure 4 where we also show the mean-squared displacement of the Pb^{2+} ions. Very long runs (0.6 ns) were required to get results of this statistical quality for the collective mean-squared displacement.

The mobility of both ionic species increases substantially across the melting transition; the F^- mobility increases by about a factor of 4, and the Pb^{2+} data are shown in the figure. The latter confirm that the Pb^{2+} ions are merely vibrating about their lattice sites in the 1300 K run, but have quite large diffusivities in the liquid at 1400 K ($\sim 5.8 \times 10^{-5}$ cm^2 s^{-1}). The

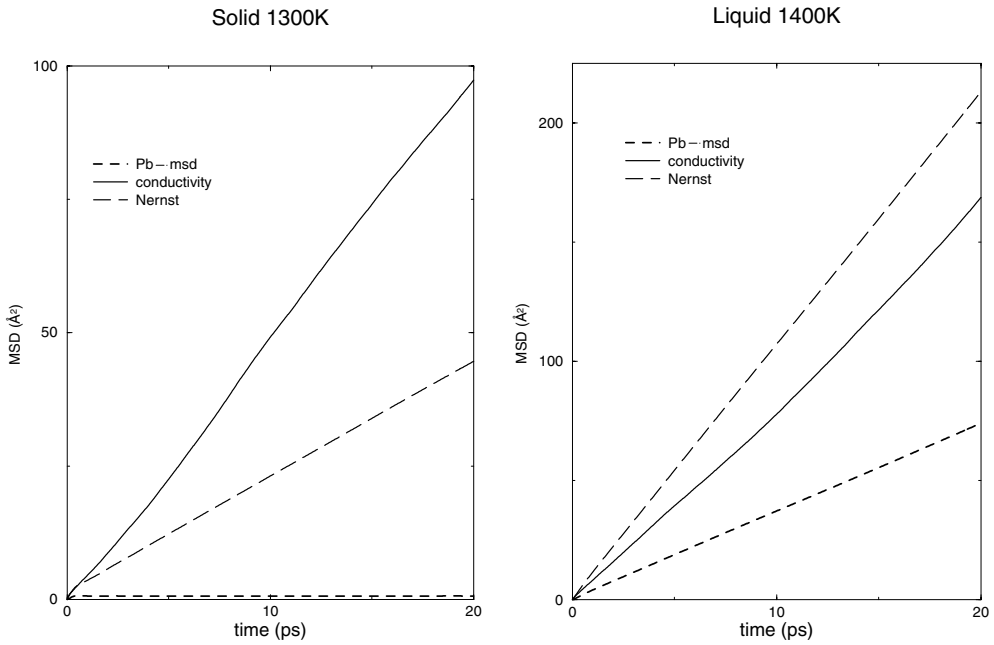

Figure 4. The collective and single particle mean-squared displacements (msd) of the ions for (a) the solid, just below the melting point, and (b) the liquid just above it. The solid line shows the collective charge msd and the slope of this line at long times gives the conductivity from equation (3.9). The long-dashed line shows the estimated charge displacement calculated from the single particle msds ignoring interionic correlations (the slope gives the Nernst–Einstein estimate of the conductivity, equation (3.11)). The short-dashed lines give the single particle msds of the Pb^{2+} ions, showing no diffusion in the solid phase and appreciable motion in the liquid.

result is that the Nernst–Einstein conductivity, predicted from the uncorrelated diffusion of the ions, increases by about a factor of 5. The true conductivity, which includes the correlation between the motion of different ions, increases by much less (by about 70%). In the liquid, the collective conductivity is slightly lower than the Nernst–Einstein value. This is typical behaviour for a strongly dissociated molten salt [25] and is normally seen as the consequence of the mutual attraction between cations and anions. For the solid, on the other hand, the collective conductivity is more than twice the Nernst–Einstein value. This indicates that the movement of the F^- ions through the Pb^{2+} is strongly correlated—it is suggestive of the collective motion of clusters of defects, or the existence of relatively long-lived diffusion pathways along which several ions move. The ratio of the Nernst–Einstein to the collective conductivity in a crystalline solid is known as Haven's ratio [26]. It can be calculated for isolated point defect models of the ionic motion (e.g. vacancy or interstitialcy models). As we shall see below, the F^- sublattice in PbF_2 close to the melting point is so strongly excited that it does not seem profitable to compare with theoretical values calculated on the basis of isolated point defects.

This observation of very different effects of correlated diffusive motion in the solid and liquid provides a rationalization for the relatively small increase of conductivity across the melting transition observed for PbF_2 [2] and other fluorite-structured superionic conductors [1].

4. Diffraction experiments and the F^- disorder

The total neutron scattering intensity is proportional to

$$S^{\mathrm{tot}}(\boldsymbol{Q}) = S_{\mathrm{PbPb}}(\boldsymbol{Q}) + 2S_{\mathrm{PbF}}(\boldsymbol{Q}) + S_{\mathrm{FF}}(\boldsymbol{Q}) \tag{4.1}$$

where

$$S_{\alpha\beta} = \langle A^*_\alpha(\boldsymbol{Q}, t) A_\beta(\boldsymbol{Q}, t)\rangle \tag{4.2}$$

and the angle brackets denote a time average. $A_\alpha(\boldsymbol{Q}, t)$ gives the instantaneous amplitude of scattering by species α at scattering vector ($\boldsymbol{Q}$):

$$A_\alpha(\boldsymbol{Q}, t) = \sum_{j=1}^{N_\alpha} b^\alpha_{\mathrm{coh}} \mathrm{e}^{\mathrm{i}\boldsymbol{Q}\cdot\boldsymbol{r}^j(t)} \tag{4.3}$$

where b^α_{coh} is the value of the scattering length for species α. In simulations, periodic boundary conditions are employed, so the only points at which scattering intensity can be calculated must satisfy

$$\boldsymbol{Q} = \frac{2\pi}{na}(l_x, l_y, l_z) \tag{4.4}$$

where a is the unit cell length of the crystal, n is the number of unit cells along a given direction of the simulation cell, and l_x, l_y and l_z are integers. The total scattering contains contributions from the time-averaged structure of the system, which is responsible for the Bragg scattering,

$$S^{\mathrm{Bragg}}(\boldsymbol{Q}) = |\langle A_{\mathrm{Pb}}(\boldsymbol{Q}, t) + A_{\mathrm{F}}(\boldsymbol{Q}, t)\rangle|^2 \tag{4.5}$$

(recall that the angle bracket denotes a time average) and from diffuse scattering, which is due to thermal and structural disorder,

$$S^{\mathrm{diff}}(\boldsymbol{Q}) = S^{\mathrm{tot}}(\boldsymbol{Q}) - S^{\mathrm{Bragg}}(\boldsymbol{Q}). \tag{4.6}$$

Both the Bragg and diffuse scattering contain information on the F^- disorder in PbF_2.

4.1. Bragg scattering and the number of F^- vacancies

For a fluorite-structured crystal, Bragg peaks are expected at scattering vectors ($\boldsymbol{k} = \frac{2\pi}{a}(m, n, p)$ with $m + n + p$ even. However, the contributions from the cation and anion sublattices to the Bragg scattering amplitude are out of phase when $m + n + p$ is not divisible by 4 [2], so that the Bragg intensity at these positions depends on the difference between the average scattering powers of the two sublattices. The neutron scattering lengths of F and Pb are in the ratio 1:1.67 (5.645 fm and 9.405 fm, respectively), so that the intensity of the $m = n = p$ peaks becomes proportional to $(n_{\mathrm{F}} - 1.67n_{\mathrm{Pb}})^2$ where n_{F} and n_{Pb} are the mean numbers of F^- and Pb^{2+} ions on their lattice sites. Since, at low temperature, $n_{\mathrm{F}} \sim 2n_{\mathrm{Pb}}$ the intensity becomes very sensitive to any variation in the occupancy of the F^- lattice sites (the Pb^{2+} ions merely vibrate about their lattice sites even in the superionic phase). Hull and co-workers [2] have exploited this sensitivity to measure the temperature variation of the number of F^- vacancies from the intensity of the (222) reflection, which is unobservably small at low temperatures but acquires appreciable intensity close to T_c.

We have calculated the (222) Bragg-peak scattering intensity in the computer simulation, using equation (4.5) and the results are shown in figure 5. Initially, the intensity drops with increasing temperature, which reflects the greater amplitude of the F^- vibration about its lattice site relative to the heavier Pb^{2+}, so that, in effect, $|n_{\mathrm{F}} - 1.67n_{\mathrm{Pb}}|$ is reduced (Debye–Waller factor). This behaviour is not seen in the experiments as the peak is too weak in

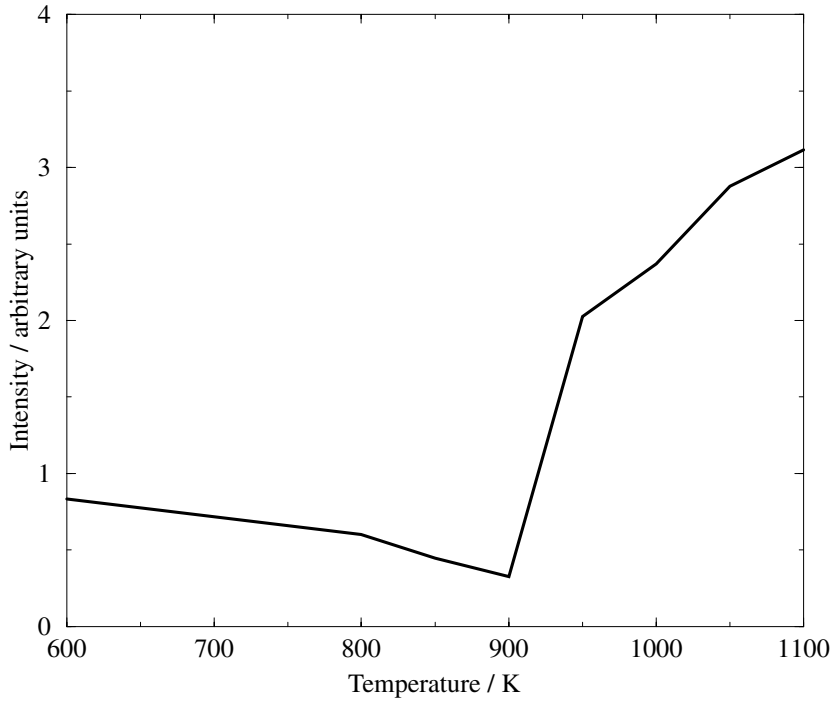

Figure 5. The intensity of the (222) Bragg peak calculated from the simulations of pure PbF_2 at different temperatures.

this temperature domain. At T_c a substantial number of the F^- ions leave their lattice sites and $|n_F - 1.67n_{Pb}|$ increases sharply and then plateaus out at still higher temperatures. This behaviour closely parallels that seen experimentally. We have also directly calculated the fraction of vacant tetrahedral F^- sites from the site occupancy analysis. The number of vacant sites begins to increase below the transition temperature due to the normal thermal excitation of isolated Frenkel pairs, before rising dramatically in a small temperature region around T_c. The number then begins to plateau. This behaviour agrees well with that of the fraction of vacant sites deduced from the experimental studies, except that the plateau value reported by Hull *et al* corresponds to about $1/4$ of the sites vacated, whereas we find a fraction closer to $1/3$. It is possible that this difference arises from the different ways in which the fraction of vacant sites is deduced, but a greater degree of disorder in the simulations could also be seen as consistent with the larger values of the rises in the heat capacity and lattice parameter reported above.

It is of interest to contrast this result, pointing to a very high degree of disordering at T_c in PbF_2, with the simulation study of CaF_2 by Gillan [16, 17]. He analysed the site occupancy above and below T_c by a different method and reported a much lower number of vacancies ($\sim$2%).

It is also interesting to combine the information that roughly 1/3 of the F^- are excited off their lattice sites across the transition with the enthalpy of the transition in order to calculate an effective enthaply for this excitation. Previously we calculated the entropy change across the transition to be 12 J K^{-1} mol^{-1} and using $T\Delta S = \Delta H$ we obtain an enthalpy change of 32.5 kJ mol^{-1} for the excitation of one mole of F^- defects. This value is considerably lower

than the Frenkel pair formation energy of 95 kJ mol^{-1} (at 700–800 K), which we estimated above from the diffusivity, and points to a high degree of cooperativity in the way that the F^- lattice becomes disordered at T_c.

4.2. Diffuse neutron scattering—structure in the disordered state

The disorder in the superionic state gives rise to appreciable diffuse scattering and this has been studied in single crystal neutron scattering for $SrCl_2$ and CaF_2, as well as PbF_2, by Hutchings *et al* [12]. Interestingly, the patterns show appreciable differences, despite the similar behaviour of the macroscopic phenomena associated with their superionicity. The diffuse scattering of interest is that due to the disorder of the anions, which will be contained within the elastic and quasielastic contributions to the total scattering. This is what is measured experimentally on a triple axis spectrometer. However, the diffuse scattering given by equation (4.6), which is readily calculated in a computer simulation, is the *total* diffuse scattering and includes inelastic scattering due to phonons. This inelastic scattering is likely to form broad features around the most intense Bragg-peak positions and appreciably affect the overall appearance of the diffuse scattering. To separate the elastic and inelastic components in the simulation would be very difficult, as it would require the spectral resolution of the dynamic structure factor at every wave vector.

We therefore resort to an approximation to compare with the diffuse scattering data. Since the scattering of interest arises from the F^- ions, we set the cation scattering length in equation (4.6) to zero. Since the Pb^{2+} ions are much heavier than the fluorides, their motion will dominate the acoustic phonon branches, so that setting the Pb scattering length to zero will largely remove the inelastic scattering from the acoustic branches.

In figure 6 we compare the diffuse scattering calculated in this way at temperatures (a) just below T_c (850 K), (b) just above T_c (950 K) and well within the superionic domain (1050 K). The most prominent feature of the experimental data [12] is a broad peak along the ⟨100⟩ direction centred at roughly (2.3, 0, 0) with a second, weaker feature along ⟨111⟩, peaking just beyond (2, 2, 2). The calculated pattern below T_c (figure 6(a)), where the F^- disorder is low, shows the residual effect of the phonon scattering. Sidebands displaced along ⟨100⟩ from the Bragg peak positions at (2, 2, 0) and (2, 2, 2) are the only regions of the scattering plane at which significant intensity is observed. Above T_c, however, a new strong feature develops at about (2.3, 0, 0) as a consequence of the disordering of the F^- ions, in good agreement with the experimental observations. The scattering around (2, 2, 2) also broadens and shifts out along the ⟨111⟩ direction, but this does not appear to have as much intensity as the experimentally recorded pattern. In the experiment, there is very little scattering close to (2, 2, 0), whereas there is a significant peak in the simulation results; however, from the below-T_c (850 K) data, we associate this with residual phonon scattering.

5. Nature of the F^- disorder in the superionic state

Our conclusion from the comparisons described above is that the simulations reproduce the experimentally observed phenomena associated with superionic behaviour sufficiently well for us to undertake a detailed examination of the F^- ion disorder in them with some confidence that this parallels that of the ions in the real material.

5.1. The spatial distribution of F^- ions

In figure 7 we contrast contour plots for the F^- ion distributions for several systems. In all cases, we see the projection of the probability distributions onto a [100] plane, so that the view

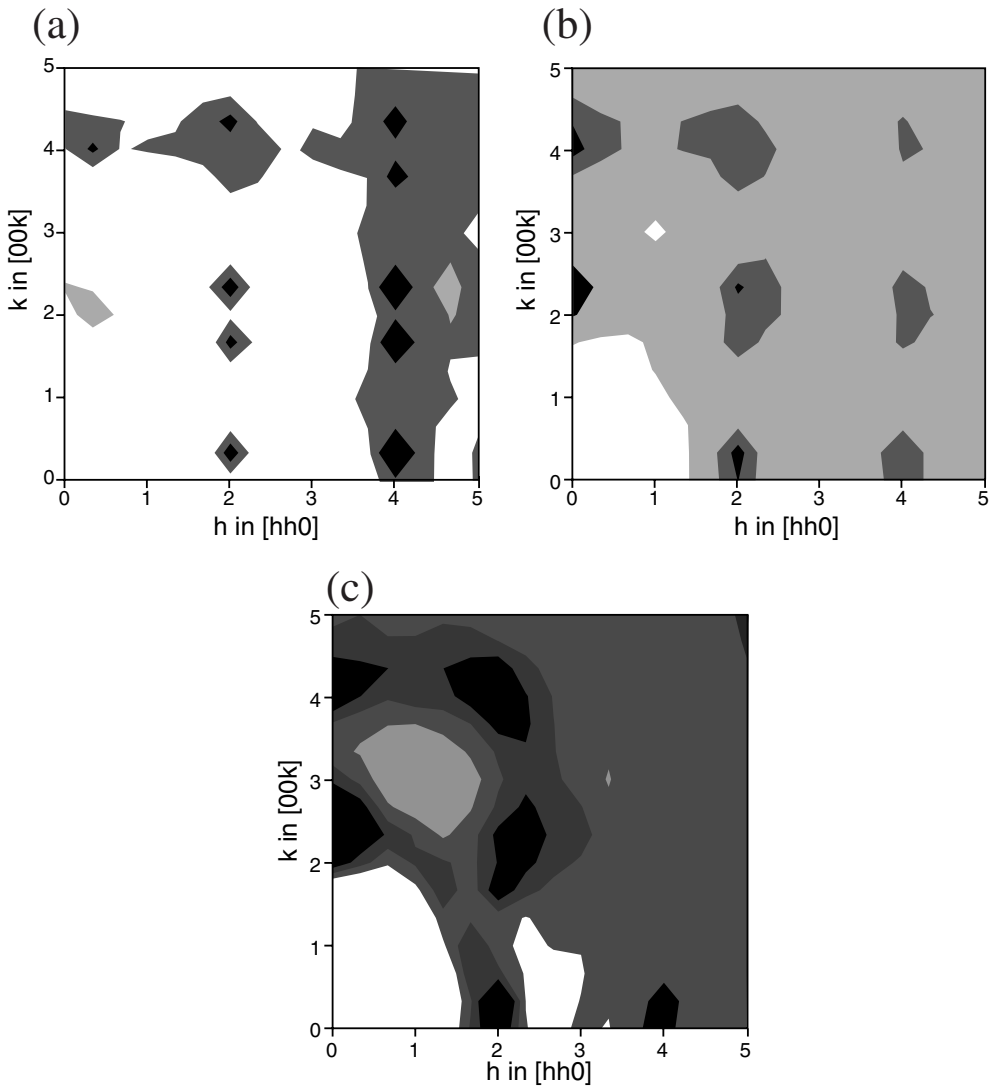

Figure 6. Diffuse neutron data calculated along the three principal crystallographic directions at (a) 850 K, (b) 950 K and (c) 1050 K, plotted versus the distance (in units of $2\pi/a_0$) along the ⟨100⟩ and ⟨110⟩ directions. Note that different contour levels are used in the three figures, the most significant feature being the growth of the diffuse scattering feature at about (2.3, 0, 0).

is dominated by peaks around the F^- ion tetrahedral sites, which form a simple cubic lattice. The Pb^{2+} ions have been omitted; had they been shown they would have appeared at the centre of each of the square cells between the F^- sites. The view shown in figure 7(a) corresponds to a 1% KF-doped system and is very similar to that obtained for the undoped crystal (not shown) at this temperature, which is below T_c for the simulation, with the F^- ions simply vibrating about their lattice sites. For the KF-doped system at this temperature there is appreciable conductivity due to the motion of the extrinsic vacancy. That this causes no apparent change in the contour plots indicates that the vacancy simply hops from lattice site to lattice site, with no significant long-lived intermediate. By contrast, in the 1% YF_3-doped system at 800 K

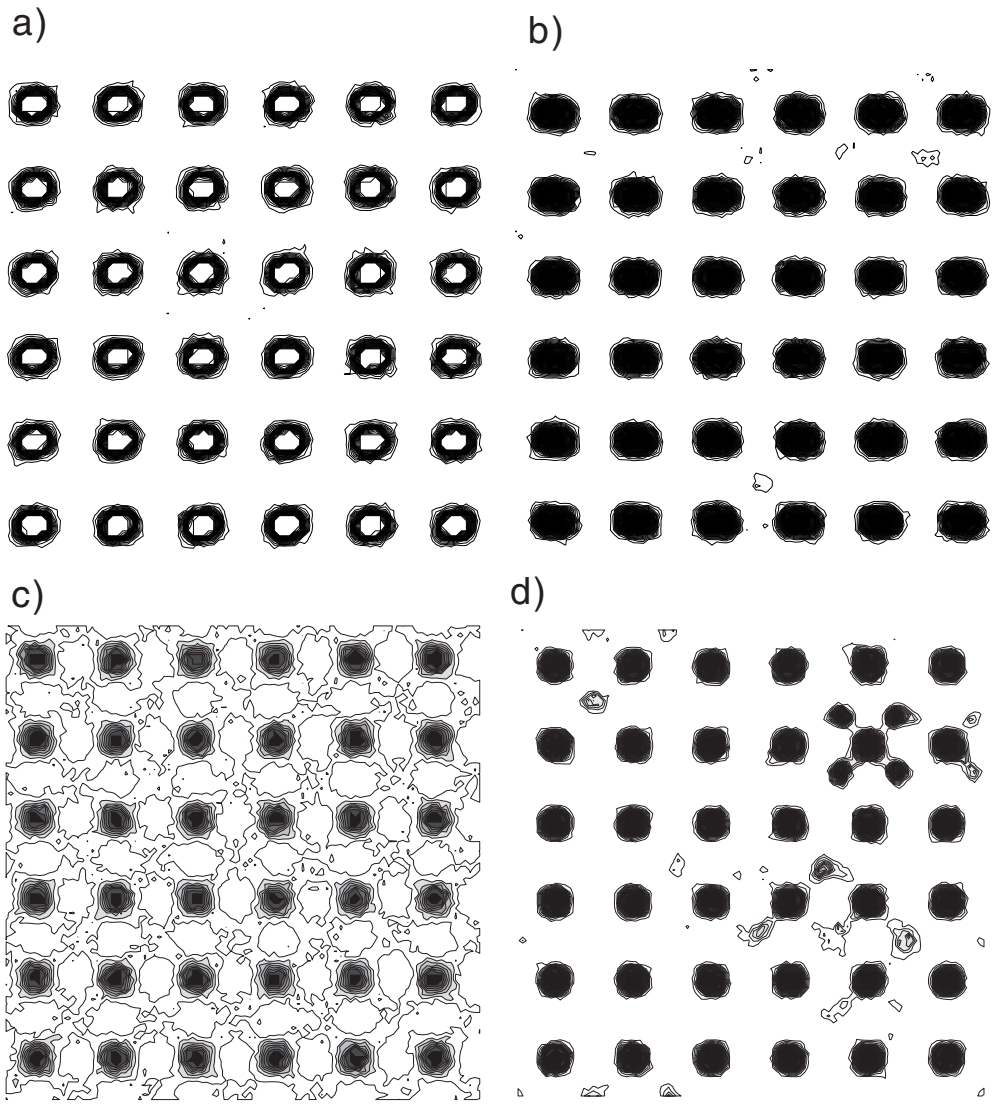

Figure 7. Contours showing the probability distributions for the fluoride ions projected in the ⟨100⟩ plane are shown for (a) the 1% KF-doped solid at 800 K, (b) the 1% YF_3-doped solid at 800 K (note the occupancy of the classical F(4) interstitial position), (c) the pure solid above the superionic transition temperature (with the F(4) site unoccupied) and (d) a 5.5% YF_3-doped system at 800 K.

(figure 7(b)), which contains a single extrinsic interstitial in the simulation cell and has a conductivity close to that of the KF-doped system, we see new features in the probability distribution which are due to the transient location of ions at several interstitial sites during the course of the run. These additional features are peaked at the centre of each square cell of the F^- lattice which corresponds to the position of the classical cube-centre interstitial F(4) site of the fluorite lattice (i.e. the octahedral hole of the close-packed Pb^{2+} lattice, see figure 1). That this classical interstitial site *is* the preferred location of the interstitial below T_c can be confirmed by several other measures.

Above T_c in the pure material (figure 7(c)), the appearance of the F^- probability distribution changes markedly. We now see significant intensity between the normal F^- lattice sites (the level of the lowest contour in this figure is some five times greater than for the (a) and (b) panels). However, this extra intensity is *not* peaked about the classical interstitial F(4) sites; in fact, the cube-centre sites are *minima* for the F^- distributions (as checked by other measures). Instead, the additional intensity appears as X-shaped extensions (in this projection) of the thermal envelope of F^- positions about their normal lattice sites. In the lightly doped samples, the contour plots above T_c are very similar in appearance to those shown in the figure, i.e. the intrinsic F^- disorder above T_c associated with the X-shaped plots swamps the effect of the extrinsic defects.

It is not possible to associate the X-shaped plots with the occupation of any other metastable F^- site within the fluorite lattice. If we rapidly quench the ionic motion to zero temperature in order to try to force the system to some local minimum, the ions merely return to their normal lattice sites no matter how rapidly the quench is undertaken. A better way of understanding the nature of the structure responsible for the X-shaped distribution is prompted by the comparison of the pure system probability distribution above T_c with that of a fairly heavily YF_3-doped system below T_c. Figure 7(d) shows the probability distribution for a 5.5% YF_3-doped system at 800 K (i.e. there are six Y^{3+} ions and therefore six extrinsic interstitials in the cell). It can be seen to exhibit similar, but more pronounced, X-shaped features to the pure superionic system. These features appear at several points across the cell, indicating that they are associated with mobile defects.

These features are the signal of interstitial clustering in the heavily doped system: that is, despite the fact that the interstitial ions carry a charge, they prefer to cluster together rather than separate under the influence of their Coulomb repulsion. These simulations were initialized from randomly chosen classical interstitial sites for the extrinsic vacancies and the Y^{3+} ions are randomly placed on the Pb^{2+} lattice. Several different startups gave very similar outcomes. The positions of the clusters seemed to bear little relationship to the Y^{3+} positions.

5.2. Interstitial clusters in the doped systems

The phenomenon of interstitial clustering is a well-established aspect of moderately doped fluorite-structured materials. It contributes to a fall-off in the conduction induced by aliovalent doping at high concentrations and has been studied with diffraction [27, 28] and NMR [29] in several materials. The preferred structures for the clusters in the simulations of the doped systems may be identified by cooling to low temperatures and examining the configurations which result. In the present simulations the preferred motif is based upon the tetrahedral arrangement illustrated in figure 8. The tetrahedron consists of three extrinsic interstitials plus a further interstitial resulting from the displacement of an F^- ion off the tetrahedral site around which the cluster is based. The cluster therefore has a net charge of -3. As illustrated in the figure the interstitials are in F(2) sites—displaced along $\langle 111 \rangle$ directions away from the central tetrahedral site so that they are about two-thirds of the way to the classical cube-centre F(4) interstitial site. We have also checked that this cluster structure persists in the simulations of the heavily (5.5%) YF_3-doped systems at temperatures of the order of 800 K by comparing the diffuse scattering pattern obtained from randomly oriented clusters with the time average diffuse scattering calculated in the simulations. At high doping levels, we also see double-tetrahedral clusters, as shown in figure 8. These involve six interstitials and two vacancies produced by F^- ions displaced from their lattice sites into interstitial sites and thus have a net

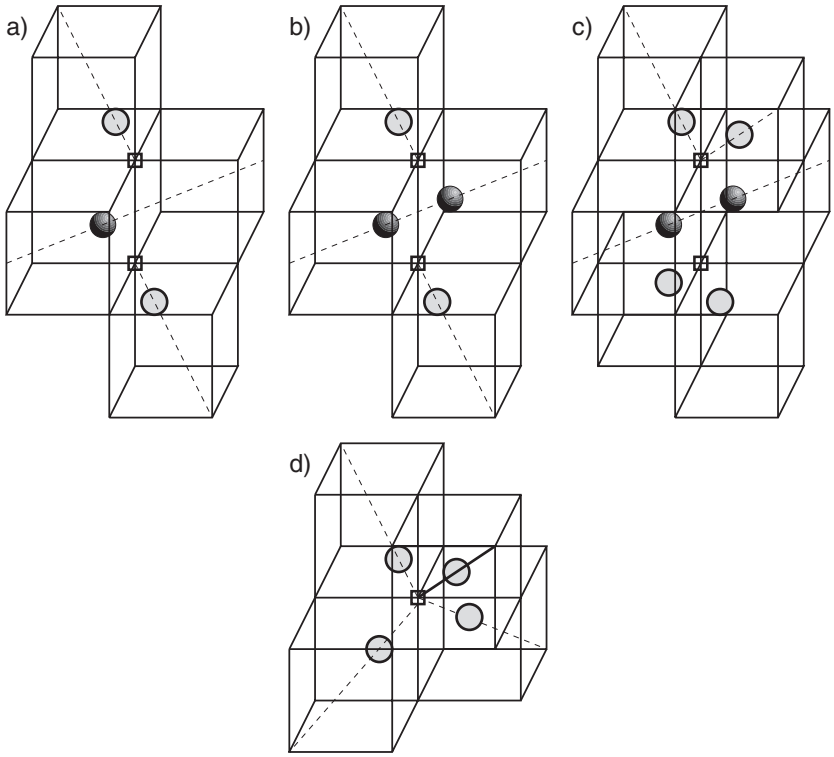

Figure 8. Four different types of cluster based on the occupation of F(1) and F(2) interstitial sites. The F(2) and F(1) sites appear as light and dark-shaded circles along the ⟨111⟩ and ⟨110⟩ vectors, respectively, and vacancies are indicated by squares on the lattice sites. (a) is the Willis cluster, (b) the ⟨110⟩ pair cluster, (c) the double tetrahedral cluster, and (d) the single tetrahedral cluster.

charge of −4. The interstitials occupy the F(1) and F(2) sites in the ratio 1:2, which is the same as observed experimentally [28].

The tetrahedral cluster may be contrasted with other structures that have been suggested for fluorite-structured materials from the analysis of diffuse scattering patterns. Hull *et al* [27] showed that the diffuse scattering in YF_3-doped CaF_2 at low temperatures was consistent with a cube octahedral structure and that this persists up to temperatures of order 500 K before dissociating. This structure also provides the best explanation of the ratio of interstitial site occupancies observed in NMR [29]. We have examined the stability of this structure in the YF_3-doped PbF_2 simulations. It can be prepared and remains metastable at low temperatures, if the Y^{3+} ions are symmetrically disposed in the immediate vicinity of the cluster to counteract the Coulombic repulsion between the interstitials, but subsequently disproportionates to form smaller clusters based upon the tetrahedron. We also examined the diffuse scattering pattern arising from the tetrahedral cluster. Although there are considerable similarities with the cuboctahedral pattern, the latter is definitely a better fit to the diffuse scattering observed in YF_3-doped CaF_2. On the other hand, Ito *et al* [28] have reported that the occupancies of interstitial sites deduced from the diffraction pattern observed in BiF_3-doped PbF_2 is not consistent with a cuboctahedral cluster and it would appear that the tetrahedral cluster, with only F(2) sites occupied, does give better agreement with the data. Another cluster relevant to our discussion is the 'Willis' cluster, illustrated in figure 8 and discussed by Hutchings

et al [12] as the best cluster model for the diffuse scattering observed in the superionic phase of PbF_2; we will discuss the relationship between this and the tetrahedral structures below.

The suggestion that emerges from this comparison of the F^- probability distributions in the pure material above T_c and the heavily YF_3-doped systems below T_c is that the superionic transition involves the collective excitation of F^- ions off their lattice sites to form transient clusters similar to those seen as stable low temperature structures in the doped systems. We will examine this relationship more closely in the next section.

5.3. Positional correlations between the defects

The similarity between the local arrangements in the heavily YF_3-doped system and in the pure material above T_c is reinforced by an examination of the correlations between the positions of the ions. Since the materials are studied at high temperature, where the ions are quite mobile, these liquid-like measures of the spatial correlations give a more reliable picture than trying to recognize particular clusters from instantaneous configurations. The site analysis program allows us to distinguish between F^- ions that lie within the tetrahedra with vertices on the Pb^{2+} sites, which correspond to the normal F^- sites of the fluorite lattice, and those which are not. The empty tetrahedral sites will be termed vacancies (V) and the ions outside these tetrahedra, interstitials (I). Note that these include any ions at the F(1) and F(2) as well as those at the classical F(4) site (which, as discussed above, has a very low probability of being occupied above T_c).

A useful measure of the spatial correlations between these defects is interstitial–vacancy (I–V) and interstitial–interstitial (I–I) coordination numbers. The I–V coordination number is the number of interstitials that are found within 3.2 Å of the vacancy site. This distance corresponds to the F–F separation in PbF_2, so that the I–V coordination number will give the number of interstitials that share a common face with the tetrahedron surrounding the site of the vacancy. A mean I–V coordination number of 1 would therefore correspond to an isolated, undissociated Frenkel pair, whereas a coordination number of 4 would correspond to the tetrahedral cluster illustrated in figure 8. The I–I coordination number gives the number of interstitials found within 4.1 Å of another interstitial. The distance was selected as the position of the first minimum in an I–I radial distribution function; note that it is substantially shorter than the distance between the centres of the nearest octahedral sites (i.e. between nearest F(4) sites) which is equal to the separation between nearest Pb^{2+} ions (4.5 Å). An isolated tetrahedral cluster would give rise to an I–I coordination number of 3.

Results for the average number of vacancies which have a particular coordination number (of interstitials) are plotted in figure 9. Figure 9(a) shows the results for YF_3-doped material at 800 K, i.e. below T_c, at various levels of doping. For low doping levels ($<2\%$), the number of vacancies (the area under the graph) is small and roughly constant. The most probable V–I coordination number is 1, indicating that the interstitial remains tightly bound to the vacancy, i.e. the vacancies appear as part of a thermally excited Frenkel pair. At higher doping levels we see an increase in the number of vacancies and in the number that are coordinated to four interstitials. That is, when the number of extrinsic interstitials in the simulation cell exceeds three, they tend to create vacancies and form tetrahedral clusters. The behaviour of the I–I coordination number probability distributions in the doped systems (figure 10(a)) is consistent with this picture. Up to a 3% doping level the predominant I–I coordination number is 0, indicating well-separated interstitials, but at higher concentrations the interstitials associate to give a distribution which is sharply peaked at 3. At the highest doping level (5.5%), the

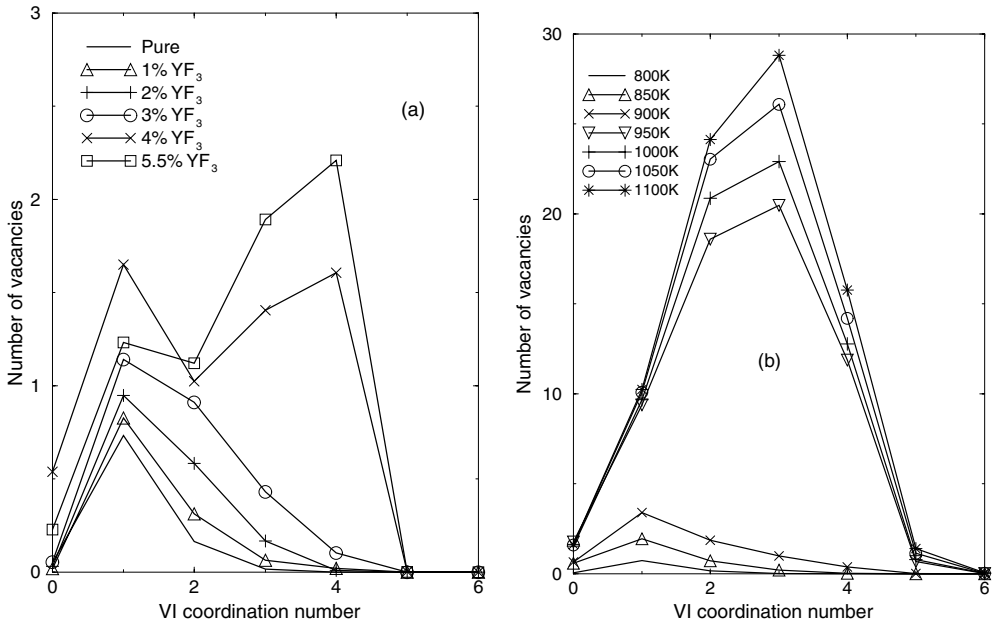

Figure 9. The distribution of vacancy–interstitial coordination numbers for (a) various YF_3-doped samples at 800 K (below the transition temperature) and (b) for pure PbF_2 at different temperatures.

average coordination numbers were consistent with the formation of the double tetrahedral cluster, illustrated in figure 8.

In figure 9(b), we compare this behaviour with that of the I–V probability distribution of the pure material as the temperature is raised through T_c. Below T_c (<950 K) we see a gradual increase in the number of bound Frenkel pairs, though there is some tendency for them to be associated, as shown by the significant number of vacancies which are close to two interstitials at 900 K. Around T_c there is a dramatic increase in the number of vacancies, as already seen in figure 5, which saturates at higher temperatures. The most probable coordination number of interstitials around the vacancies is 3; apart from this point of detail, the thermal behaviour of the pure system is remarkably similar to that of the doped system with increasing concentrations of extrinsically introduced interstitials. The high temperature pure system I–I distribution (figure 10(b)) is somewhat broader than that of the doped system (figure 10(a)), and indicates a higher degree of association as the temperature is raised to 1100 K.

The degree of disorder of the F^- ions above T_c is very high, with about 30% of the F^- ions displaced from their lattice sites and associated with a high degree of mobility (fluidity). As such, it should be described in terms of particular local structural motifs (i.e. clusters) with care—a liquid-like viewpoint is more reliable. However, since diffuse scattering results tend to be interpreted in terms of clusters it is perhaps appropriate to reduce the information in the figures to these terms. A comparison of the highly probable coordination numbers in the simulations with those that would be predicted from the various cluster structures shows that the data are consistent with a roughly equal mixture of the ⟨110⟩ pair clusters and the double tetrahedral cluster. Both involve two vacancies on adjacent sites. The ⟨110⟩ pair cluster has a charge of -2, and has two F^- ions on F(2) and two on F(1) sites. Catlow and Hayes [5]

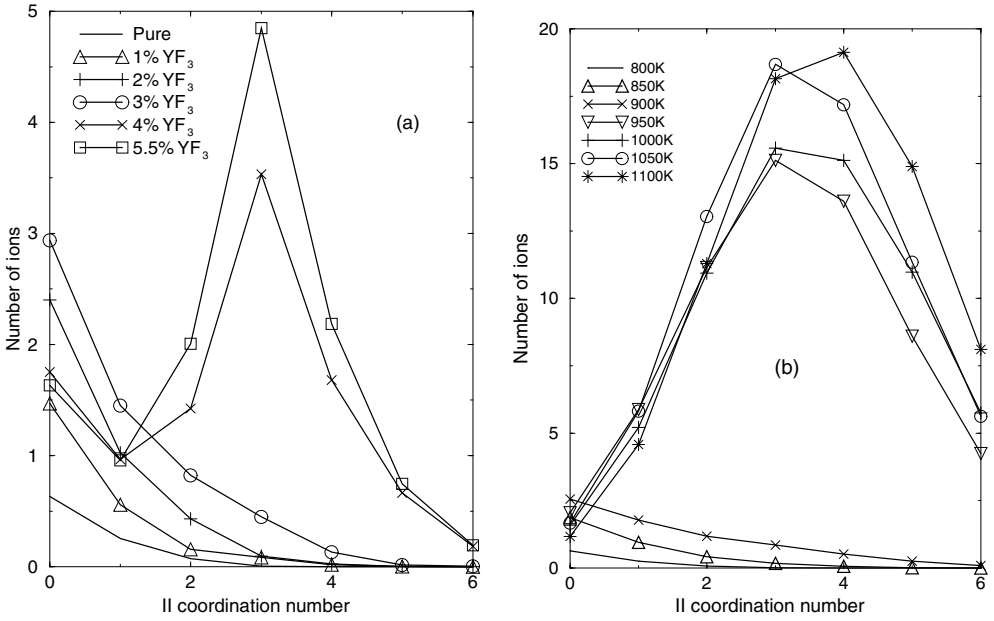

Figure 10. The distribution of interstitial–interstitial coordination numbers for (a) various YF_3-doped samples at 800 K (below the transition temperature) and (b) for pure PbF_2 at different temperatures.

showed that there was a barrier to recombination for this cluster in a low temperature lattice. The double tetrahedral cluster has a charge of -4, which must be balanced by vacancies elsewhere in the lattice and twice as many ions associated with F(2) compared to F(1) sites. Hutchings *et al* [12] interpreted their diffuse scattering results in terms of the Willis cluster, which has the same proportion of F(2) to F(1) sites and equates to half the double tetrahedral cluster.

6. Conclusions

The polarizable ion simulation potential has been shown to reproduce, semi-quantitatively, many of the observable properties associated with the transition of PbF_2 to superionic behaviour. Included in the study has been the effect of aliovalent doping on the conductivity of β-PbF_2, which can be contrasted with our earlier examination of this effect in the 'non-conducting' α phase [7]. In the study of conductivity, we have provided an explanation for the similarity of the values of conductivity above and below melting, which is a frequently observed phenomenon in superionic materials. In the crystal, the motions of individual ions are strongly correlated, resulting in a conductivity which is more than twice that estimated from the Nernst–Einstein formula. After melting, the individual ionic mobilities do increase substantially, but the correlations become slightly negative, as is typical for a molten salt, so that the anticipated large jump in conductivity does not occur.

The principal purpose of the paper was to examine the nature of the disorder in the superionic phase. We have shown that the disorder in the simulations is consistent with the diffraction and diffuse scattering information on PbF_2 [6, 12]: perhaps the greatest limitation

on the comparison with diffuse scattering is the difficulty of fully eliminating the inelastic contributions in the simulations. The simulations show that the transition to superionic behaviour is associated with the excitation of a very large fraction of the F^- ions off their lattice sites (in agreement with the experimental analyses). On this our results differ markedly from those of Gillan who studied the related material CaF_2 [16, 17] with an effective pair potential and reported only a small fraction displaced: whether this is due to the material, the interaction potential or the method of structural analysis is, at present, unclear. In our calculations, the displaced ions are found in the vicinity of F(1) and F(2) interstitial sites (see figure 1), in agreement with experiment, and not at the classical cube-centre F(4) interstitial site of the fluorite lattice.

The collective excitation appears as a consequence of an attractive effective interaction between interstitial ions, which results in pronounced spatial correlations between the interstitial ions and vacancies in the superionic phase. These correlations seem to be much stronger than could arise from the mean-field Coulombic interaction recently studied by Maier and co-workers [9]. The local ordering is similar (but not identical) to that found in the interstitial clusters formed by moderately doping PbF_2 with YF_3. Since the latter can be formed at low temperatures, their structures may be fully characterized. The origins of the effective attraction will be studied in future work.

Acknowledgments

We are grateful to Mark Wilson for assistance with the simulations and to Clare Grey (SUNY, Stony Brook) and Steve Hull (Rutherford Laboratory) for stimulating discussions and for sending data. The work was supported by EPSRC grant through GR/L/49369 and a studentship for MJC.

References

[1] Chandra S 1981 *Superionic Solids. Principles and Applications* (Amsterdam: North-Holland)
[2] Hull S, Berastegui P, Eriksson S G and Gardner N J G 1998 *J. Phys.: Condens. Matter* **10** 8429
[3] Andersen N H, Clausen K and Kjems J K 1983 *Solid State Ionics* **9–10** 543
[4] Goff J P, Hayes W, Hull S and Hutchings M T 1991 *J. Phys.: Condens. Mattter* **3** 3677
[5] Catlow C R A 1980 *Comment. Solid State Phys.* **9** 157
Catlow C R A and Hayes W 1982 *J. Phys. C: Solid State Phys.* **15** L9
[6] Hull S and Keen D A 1998 *Phys. Rev.* B **58** 14837
[7] Castiglione M J, Wilson M, Madden P A and Grey C P 2001 *J. Phys.: Condens. Matter* **13** 51
[8] Liang C C and Joshi A V 1975 *J. Electrochem. Soc.* **122** 466
[9] Hainovsky N and Maier J 1995 *Phys. Rev.* B **51** 15789
[10] Zimmer F, Ballone P, Parrinello M and Maier J 2000 *Solid State Ionics* **127** 277
[11] Hiernaut J P, Hyland G J and Ronchi C 1993 *Int. J. Thermophys.* **14** 259
Hiernaut J P, Hyland G J and Ronchi C 1993 *Int. J. Thermophys.* **14** 609
[12] Hutchings M T, Clausen K, Dickens M H, Hayes W, Kjems J K, Schnabel P G and Smith C 1984 *J. Phys. C: Solid State Phys.* **17** 3903
[13] Dickens M H and Hutchings M T 1978 *J. Phys. C: Solid State Phys.* **11** 461
[14] Walker A B, Dixon M and Gillan M J 1982 *J. Phys. C: Solid State Phys.* **15** 4061
[15] Jaccucci G and Rahman A 1978 *J. Chem. Phys.* **69** 4117
[16] Gillan M J 1986 *J. Phys. C: Solid State Phys.* **19** 3391
[17] Gillan M J 1986 *J. Phys. C: Solid State Phys.* **19** 3517
[18] Wilson N T, Wilson M, Madden P A and Pyper N C 1996 *J. Chem. Phys.* **105** 11209
[19] Castiglione M J, Wilson M, Madden P A and Pyper N C 1999 *J. Phys.: Condens. Matter* **11** 9009
[20] Chaudhuri S, Castiglione M J, Wang F, Wilson M, Madden P A and Grey C P *Mat. Res. Bull.* submitted
[21] Fowler P W and Madden P A 1984 *Phys. Rev.* B **29** 1035

[22] Fowler P W and Pyper N C 1985 *Proc. R. Soc.* A **398** 377
[23] Pyper N C 1986 *Phil. Trans. R. Soc.* A **320** 107
[24] Martyna G J, Tobias D J and Klein M L 1994 *J. Chem. Phys.* **101** 5
[25] Hansen J-P and McDonald I R 1986 *Theory of Simple Liquids* (New York: Academic)
[26] Kompaan K and Haven Y 1956 *Trans. Faraday Soc.* **52** 786
Kompaan K and Haven Y 1958 *Trans. Faraday Soc.* **54** 1498
[27] Hull S and Wilson C C 1992 *J. Solid State Chem.* **100** 101
[28] Ito Y, Koto K, Yoshikado S and Ohachi T 1986 *Solid State Ionics* **18–19** 1202
[29] Grey C P and Wang F 1995 *J. Am. Chem. Soc.* **117** 6637